Full length article

# Correlations of grain boundary segregation to sintering techniques in a three-phase ceramic

Komal Syed [a],[*], Mingjie Xu [a],[b], Kenta K. Ohtaki [a], David Kok [a], Keyur K. Karandikar [c], Olivia A. Graeve [c], William J. Bowman [a], Martha L. Mecartney [a]

[a] *Department of Materials Science & Engineering, University of California Irvine, Irvine, CA, USA*
[b] *Irvine Materials Research Institute, University of California Irvine, Irvine, CA, USA*
[c] *Department of Mechanical and Aerospace Engineering, University of California San Diego, La Jolla, CA, USA*

A B S T R A C T

The effects of using different sintering techniques (conventional, flash and spark plasma sintering) on grain boundary segregation were investigated in a 3-phase polycrystalline ceramic containing cubic 8 mol% $Y_2O_3$ stabilized $ZrO_2$ (YSZ), $\alpha$-$Al_2O_3$ and $MgAl_2O_4$. Six types of interfaces for each sintered sample were analyzed for grain boundary chemistry. Using aberration-corrected STEM and EDS, we show Al segregation at YSZ-YSZ boundaries, and Y/Zr segregation at $Al_2O_3$-$Al_2O_3$, $MgAl_2O_4$-$MgAl_2O_4$ and $MgAl_2O_4$-$Al_2O_3$ boundaries. YSZ-$MgAl_2O_4$ and YSZ-$Al_2O_3$ heterointerfaces, in contrast, do not show elemental segregation. Our results show that the type of segregation at different boundaries does not change with different sintering processes, indicating that elemental segregation mainly depends on initial sample composition, although the amount of segregation can vary. Quantitative analyses reveal that spark plasma sintering (950°C for 5 min, 100 MPa) results in relatively higher average segregation at grain boundaries and heterointerfaces compared to conventional sintering (1550°C for 10 h), suggesting that low temperatures result in higher grain boundary segregation. The average segregation concentrations at the grain boundaries of our flash sintered sample (estimated to reach 1700°C for 6 s) were found to be consistently similar to long-annealed spark-plasma sintered sample (1350°C for 20 h), suggesting that very high temperatures reached during flash process can achieve similar segregation concentrations compared to a SPS sample annealed for several hours at lower temperature. The presence of other phases in multi-phase systems can modify the grain boundary chemistry and segregation compared to segregation in single-phase ceramics.

## 1. Introduction

Grain boundaries play a critical role in engineering materials in terms of their material properties, such as thermal conductivity, fracture strength, high temperature creep, corrosion, electrical, chemical and magnetic properties [1–8]. Grain boundaries can be considered 2D defects that have excess free energy. Understanding the elemental segregation at grain boundaries and point defect generation in bulk can provide practical processing knowledge for desirable properties using grain boundary engineering [9,10]. While there are many similarities between grain boundary characteristics of metals and ceramics, the ionic character of ceramic grain boundaries and complex crystal structures in ceramics add a further degree of complexity [4,11]. Since the applications and integrity of ceramics depend highly on the chemistry of these defects, significant research has been done to analyze grain boundary segregation behavior in ceramics [4,11].

Bulk ceramic processing includes the densification of powders at high temperatures. Different ceramic processing techniques have been developed and are still developing to fully densify ceramics in shorter times and lower temperatures, such as with the application of electric field and pressure, for energy and cost savings [12–17]. However, these changes in processing techniques can have a significant impact on the composition, structure and stability of the grain boundaries. For instance, elemental segregation at grain boundaries and point defect generation in the bulk can serve to disrupt phonon propagation, reducing thermal conductivity [18,19]. Goel *et al.* [9] concluded that the increased clustering of segregated atoms at the grain boundaries result in major local disorder which is the primary reason behind increase in thermal grain boundary (Kapitza) resistance. Furthermore, correlations between grain boundary chemistry and mechanical properties, such as fracture toughness, have been widely studied [20–23]. Thus, any change in grain boundary segregation can have a significant effect on material properties.

* Corresponding author.
  *E-mail address:* ksyed1@uci.edu (K. Syed).

While the grain boundary segregation behavior has been explored widely for different ceramic systems, most studies to date have been focused on bicrystals or single-phase polycrystalline ceramics with added dopants [8,24–29]. Furthermore, most of such studies focus on qualitative observations of grain boundary segregation or relation to various material properties, whereas quantitative segregation analyses are limited. Several factors can affect the segregation behavior in ceramics such as point defect interactions, impurity/dopant cation size, grain boundary energy, and electrostatic interactions [11]. Segregation chemistry varies considerably even between undoped and doped single phase ceramics. For instance, Y segregation is widely observed at YSZ grain boundaries explained by classical space charge theory [24,30–32]; but when YSZ is doped with $Al_2O_3$, both Al and Y segregation have been observed [33]. However, *multiphase* engineering ceramics have more interface diversity, and contain more complicated heterointerfaces. Moreover, various ceramic processing techniques create additional and distinct complexity in understanding grain boundary segregation. Based on findings from previous literature, and the variety of factors which could affect segregation, we hypothesize that grain boundary segregation in multiphase ceramics can be quite distinct compared to their single-phase counterparts, because of the presence of other phases in the system that act as infinite sources of ions to segregate at grain boundaries. Thus, exploring this experimentally will address a significant gap in understanding how different sintering processes affect the grain boundaries in technical ceramics.

In this study, we report direct observation of segregation at grain boundaries for a three-phase polycrystalline ceramic $Al_2O_3$ – $MgAl_2O_4$ – YSZ using aberration-corrected STEM-EDS. The model ceramic system chosen for this study consists of phases which are all widely used engineering ceramics, commercially available as both powders and single crystals, are chemically stable and do not form any secondary phases. This study explores the correlations, both qualitative and quantitative, between grain boundary segregation behavior and different sintering techniques: (1) conventional sintering, (2) flash sintering [16], and (3) spark plasma sintering (SPS) [17]. In addition, the effects of annealing times after SPS sintering on grain boundary segregation are discussed.

## 2. Experimental methods

### 2.1. Sample preparation

#### 2.1.1. Conventional sintering

Starting powders of 8 mol% yttria stabilized zirconia or YSZ ($Y_{0.08}Zr_{0.92}O_2$, TZ-8YS Tosoh), $Al_2O_3$ (TM-DAR Taimei) and $MgAl_2O_4$ (S30CR Baikowski) were used in equal amount by volume (33 vol%). The powders were attrition milled for ~8 h and the slurry was dried overnight at 100°C. Mortar and pestle were used to break any agglomerates. The mixed powder was pressed using a cold isostatic press at 55 kpsi for 5 min, and the green body was sintered at 1550°C for 10 h in air with heating rate of 10°C/min. Using the Archimedes displacement method, the density was measured to be 97%. The average grain size was 1 μm for this sample.

#### 2.1.2. Flash sintering

Processing details of flash sintered sample were published previously [13,34]. The furnace was heated to 1450°C using a constant rate of 10°C/min. Flash sintering experiments were performed at an applied electric field of 650 V/cm with a 6 s current hold at 50 mA/mm². The electric field and current density were constant throughout the process. Kok *et al.* [34] reported using in-situ data that the actual sample temperature was much higher (~1700°C) than the furnace temperature during the flash sintering experiment, due to significant Joule heating produced by the current flowing through the sample. The average grain size of this sample was 230 nm.

**Table 1**
Calculated k-factors using standard powders.

| Standard Powder | Element ratio | Experimental k-factors |
|---|---|---|
| $MgAl_2O_4$ | Mg:Al | 1.08 ± 0.04 |
| YSZ | Y:Zr | 0.81 ± 0.06 |
| $Y_3Al_5O_{12}$ | Al:Y | 0.57 ± 0.01 |

#### 2.1.3. Spark plasma sintering

Two different SPS samples were prepared for this study, as reported previously [35]. Both SPS samples were sintered at 950°C for 5 min using heating rate of 100°C/min under 100 MPa. The first sample was annealed at 1000°C for 1 h to remove carbon contamination which is typical during SPS process; this sample will be referred as 'SPS' from this point. The SPS sample had an average grain size of 260 nm. The second sample went through prolonged annealing of 20 h at 1350°C after sintering, to allow for grain growth. This sample will be referred to as 'SPS anneal' for the rest of the paper. The average grain size of the SPS anneal sample was 690 nm.

All sintered samples were coated with 5–7 nm of carbon coating using a Leica sputter coater. TEM samples were prepared by the lift-out method using a Tescan GAIA3 SEM integrated with focused ion beam (FIB).

### 2.2. Scanning transmission electron microscopy (STEM) - Energy dispersive X-ray spectroscopy (EDS) characterization

Grain boundaries were analyzed using an aberration-corrected STEM operated at 300 keV (JEOL Grand ARM300CF). This instrument is equipped with dual silicon drift detectors for energy dispersive x-ray spectroscopy (EDS) with total detector area of 200 mm². STEM-EDS mapping and spot analysis were applied using the following EDS peaks: O ($K_\alpha$ at 0.52 keV), Mg ($K_\alpha$ at 1.25 keV), Al ($K_\alpha$ at 1.49 keV), Y ($K_\alpha$ at 14.95 keV and $K_\beta$ at 16.74 keV) and Zr ($K_\alpha$ at 15.78 keV and $K_\beta$ at 17.67 keV). The probe size was ~0.1 nm with a probe current of ~35 pA. A low-background, high count analytical TEM holder was used to minimize any stray x-rays caused by the holder. Gatan Microscopy Suite (GMS version 3) software was used. Net counts for EDS elemental maps were obtained after background subtraction using Kramers filter (with scaling option available in GMS to better align the measured background to the original data). The EDS parameters were optimized based on minimizing beam damage versus increasing net EDS counts.

The quantification of elemental segregation at the grain boundaries was performed using the Cliff-Lorimer method [36,37]. EDS maps were acquired close to the midpoint of the grain boundaries between triple junctions, over ~12–15 min per boundary using step sizes close to the probe size ~0.1 nm. Due to the widely known limitations of quantification of light elements (O or below) using EDS, only quantification of cations (Mg, Al, Y and Zr) was completed for grain boundary compositional analysis in this paper. The k-factors ($k_{Mg-Al}$, $k_{Y-Zr}$ and $k_{Al-Y}$) were calculated using experimental spot EDS data of standard powders $MgAl_2O_4$, 8YSZ, and $Y_3Al_5O_{12}$ (>99% purity) respectively. The dwell time per spot was 150 seconds to ensure a high number of counts for reliable quantification. The same background subtraction method was used as mentioned earlier for the 3-phase samples. These three standard powders were selected because they have a known composition and each standard relates two of the elements of interest in our 3-phase system. Unlike Mg/Al and Y/Zr which are close in atomic number, Al/Y is expected to have a large difference in absorption correlated with thickness effects [38,39]. Therefore, we determined experimental $k_{Al-Y}$ value (from Cliff-Lorimer equation) using $Y_3Al_5O_{12}$ powder particles of similar estimated thickness to our TEM samples, ~100-110 nm. All experimental k-factors (mean value and one standard deviation) are provided in Table 1.
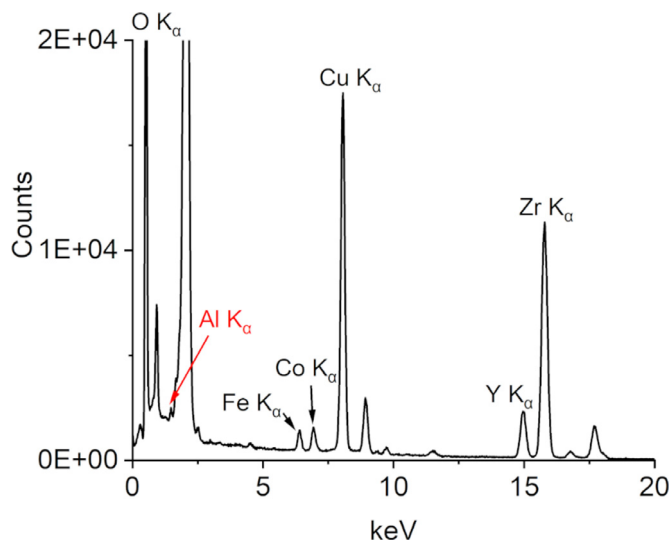
**Fig. 1.** EDS spectrum of YSZ powder (with marked Kα peaks only) showing Al artifact peak marked with red arrow. The y-axis (counts) has been cropped for visibility of the small Al peak.



**Fig. 2.** Y and Zr concentration profiles across an alumina-alumina grain boundary in conventional sintered sample.

A small Al signal was observed in the EDS spectra of YSZ powder (Fig. 1), which was determined to be an Al artifact. This Al artifact signal was further confirmed using a hole count test. Fe was also consistently observed in the EDS spectra, coming from the microscope column. The Al EDS quantification artifact was corrected for all grain boundaries analyzed in all samples of this study. This was done by calculating an average Fe/Al net count ratio from ten EDS spot spectra obtained from YSZ powder, and subtracting the Al signal (via the Fe signal) from spectra measured on our experimental specimens.

To survey multiple variants of boundaries in the samples analyzed, 2–5 grain boundaries of each type were characterized in each sample. Grain boundaries were tilted to be parallel to the electron optic axis prior to STEM-EDS data acquisition. Electron channeling effects were ignored from our chemical analysis.

Besides the Cliff-Lorimer method for quantitative compositional analysis (in atomic%), grain boundary segregation is often expressed using grain boundary coverage or chemical excess (in atoms/nm$^2$). This chemical excess at grain boundaries can be calculated using the spatial difference technique, where the segregant's EDS signal acquired in the grain is subtracted from its signal acquired from the grain boundary. This is described in detail by Sternlicht *et al.* [39]. Here, the grain and grain boundary EDS signals used in the spatial difference technique were acquired using EDS mapping data (thickness effect for different grain boundaries characterized was not considered). The chemical excess was calculated using the following equation [39–42]:

$$\Gamma = \frac{V}{S} \frac{A_B}{A_A} \rho k_{AB} \frac{I_A}{I_B} \quad (1)$$

where, V/S is the ratio between interaction volume to area of the grain boundary of interest; this ratio can be simplified and equals the width of the scan (nm) perpendicular to the grain boundary [39]. $\rho$ is the site density (atoms/nm$^3$) of selected element in the grain. $A_A$ is the atomic weight of excess species and $A_B$ is the effective atomic weight of selected element in the grain (same element used for density); $A_B/A_A$ is unitless. $I_A$ and $I_B$ are the intensities of excess species (minus the intensities from adjacent grains) and the matrix element selected. Eq. (1) used in this work assumes all segregating atoms are lying on a monolayer, which removes the variance in grain boundary width and if grain boundaries are not exactly parallel with the electron optic axis. The calculated excess amount thus reflects the whole grain boundary because we have integrated the segregant concentrations from the whole grain boundary
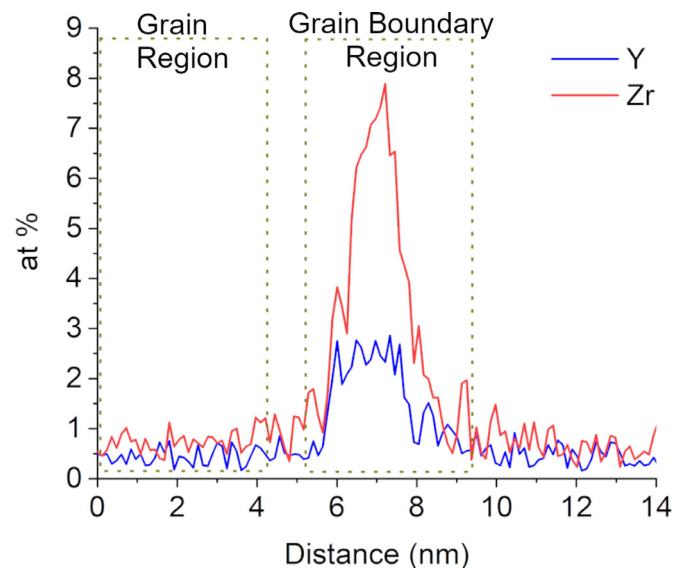
width and then substracted the contribution from the bulk using same width.

Eq. (1) was modified for each of the homointerfaces based on the observed segregants as well the chemistry of the grains neighboring the interfaces. The product of k-factor and intensity ratio from Eq. (1) was converted to concentration ratio (based on the Cliff-Lorimer equation). Eq. (2) is the modified equation for calculating Zr excess at alumina-alumina grain boundaries:

$$\Gamma = \frac{V}{S} \frac{2A_{Al}}{A_{Zr}} \rho_{Al}^G \frac{C_{Zr}^{GB} - C_{Zr}^G}{C_{Al}^G} \quad (2)$$

where, supercripts G and GB stand for grain and grain boundary, respectively. $\rho_{Al}^G$ is the site density of Al in alumina grain, $C_{Zr}^{GB}$ is the concentration of Zr at the grain boundary, $C_{Zr}^G$ is the concentration of Zr in the alumina grain and $C_{Al}^G$ is the concentration of Al in the alumina grain. Y/Zr concentration profiles across an alumina-alumina grain boundary in conventional sintered sample is given in Fig. 2. 'Grain boundary region,' marked in Fig. 2, is used to obtain concentration data of Y and Zr segregated species ($C_Y^{GB}$ and $C_{Zr}^{GB}$ respectively) and marked 'grain region' is used to obtain concentration of Al in the grain ($C_{Al}^G$) and concentration of Y and Zr in the grain ($C_Y^G$ and $C_{Zr}^G$ respectively).

For spinel-spinel grain boundaries, Al is selected as the matrix metal ion for chemical excess calculations, similar to alumina-alumina grain boundaries. For YSZ-YSZ grain boundaries, Zr is selected as the matrix metal ion.

In order to better understand the grain boundary segregation behavior, we also analyzed the estimated concentrations of cations within the phases using EDS spot analysis. To analyze the concentrations of Mg and Al cations within the YSZ grains, EDS spot analysis was performed and averaged for 8 grains. Similarly, for Y and Zr concentrations in alumina and spinel phases, spot analysis was averaged for 3 grains since Y/Zr are known to have very limited solubility in those phases.

## 3. Results and discussion

### 3.1. Qualitative observations of elemental segregation at grain boundaries

Fig. 3(a) shows the schematic of a model 3-phase sintered ceramic composed of alumina, spinel and YSZ. Fig. 3(b) shows a bright-field (BF) TEM image of SPS anneal sample showing all the homointerfaces (grain boundaries between like phases) and heterointerfaces (grain boundaries between
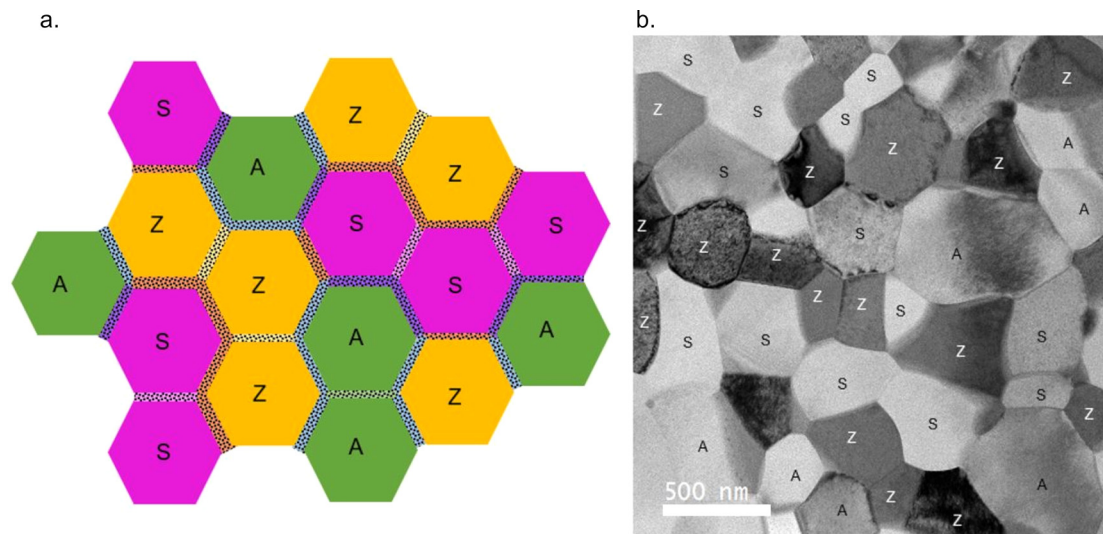
**Fig. 3.** (a) Schematic diagram showing six types of grain boundaries in a three-phase sintered ceramic containing $MgAl_2O_4$, $Al_2O_3$, and YSZ. (b) Bright field-TEM image of SPS anneal sample with average grain size of ~690 nm. S = Spinel, A = Alumina, Z = YSZ.
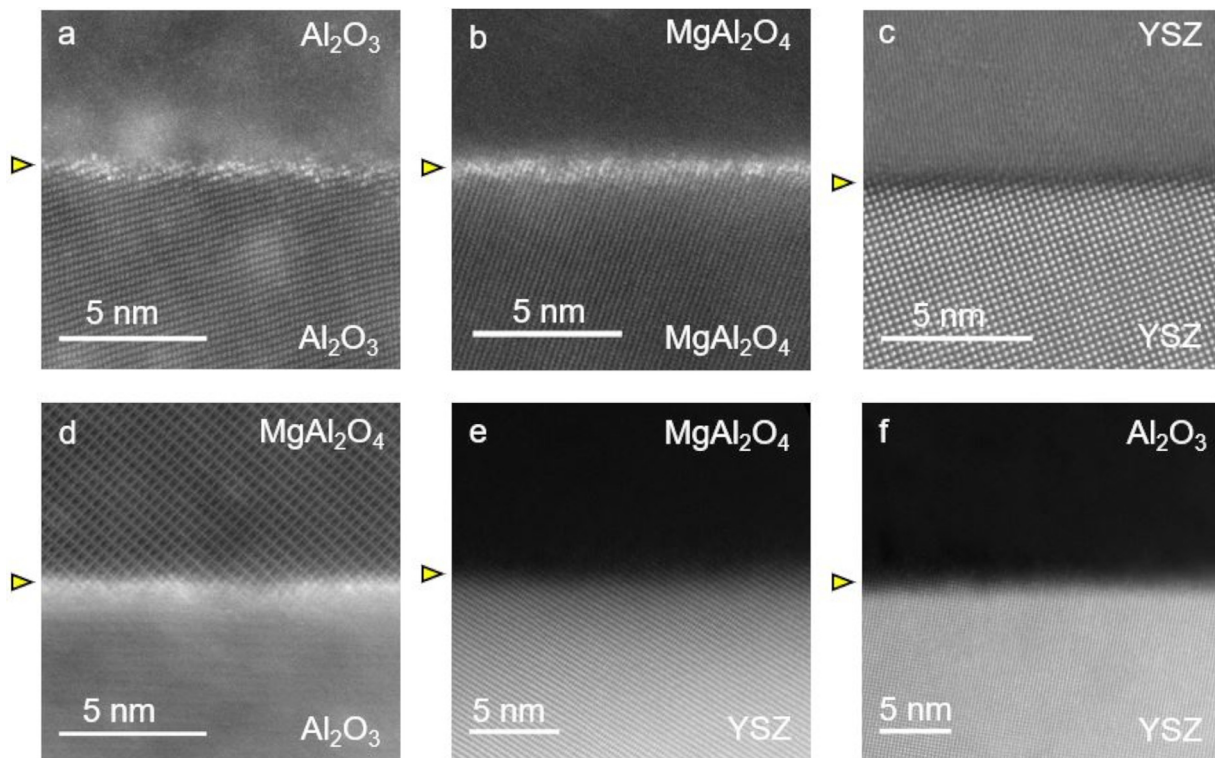


**Fig. 4.** STEM HAADF images of different types of grain boundaries in the 3-phase sintered ceramics. (a) $Al_2O_3$-$Al_2O_3$ in SPS anneal, (b) $MgAl_2O_4$-$MgAl_2O_4$ in conventional sintered, (c) YSZ-YSZ in flash sintered, (d) $MgAl_2O_4$-$Al_2O_3$ in SPS anneal, (e) YSZ-$MgAl_2O_4$ in conventional sintered and (f) YSZ-$Al_2O_3$ in SPS. Bright contrast at grain boundaries indicates segregation of higher atomic number (Z) elements (a,b,d) while dark contrast at grain boundaries indicates segregation of lighter Z elements (c). The arrows mark the grain boundary location.

between dissimilar phases) observed in our 3-phase system. Considering the four kinds of sintered samples used for this study, a total of 24 types of interfaces are investigated for chemical analysis (i.e. six interfaces for each of conventional, flash, SPS and SPS anneal samples). Fig. 4 shows STEM high-angle annular dark field (HAADF) images of the six types of boundaries observed in each sample. Fig. 4a-b,d show high intensity contrast at the grain boundaries indicating presence of higher Z elements at spinel-spinel, alumina-alumina and spinel-alumina grain boundaries (STEM HAADF image intensity is proportional to atomic

number Z [43]). The YSZ-YSZ interface in Fig. 4c, on the other hand, shows darker contrast at the grain boundary; the dark contrast could be due to lower Z elements but also common due to structural distortion at grain boundaries caused by charge-compensating anion vacancies [44,45]. On the other hand, YSZ-spinel and YSZ-alumina heterointerfaces do not show any segregation. This is an interesting observation because segregation is known to occur at other heterointerfaces, such as metal-ceramic systems like Cr-doped Ni/YSZ [46], MgO/Cu(Ag) [47], Al alloy-$B_4C$ [48]. In most of such interfacial segregation stud-
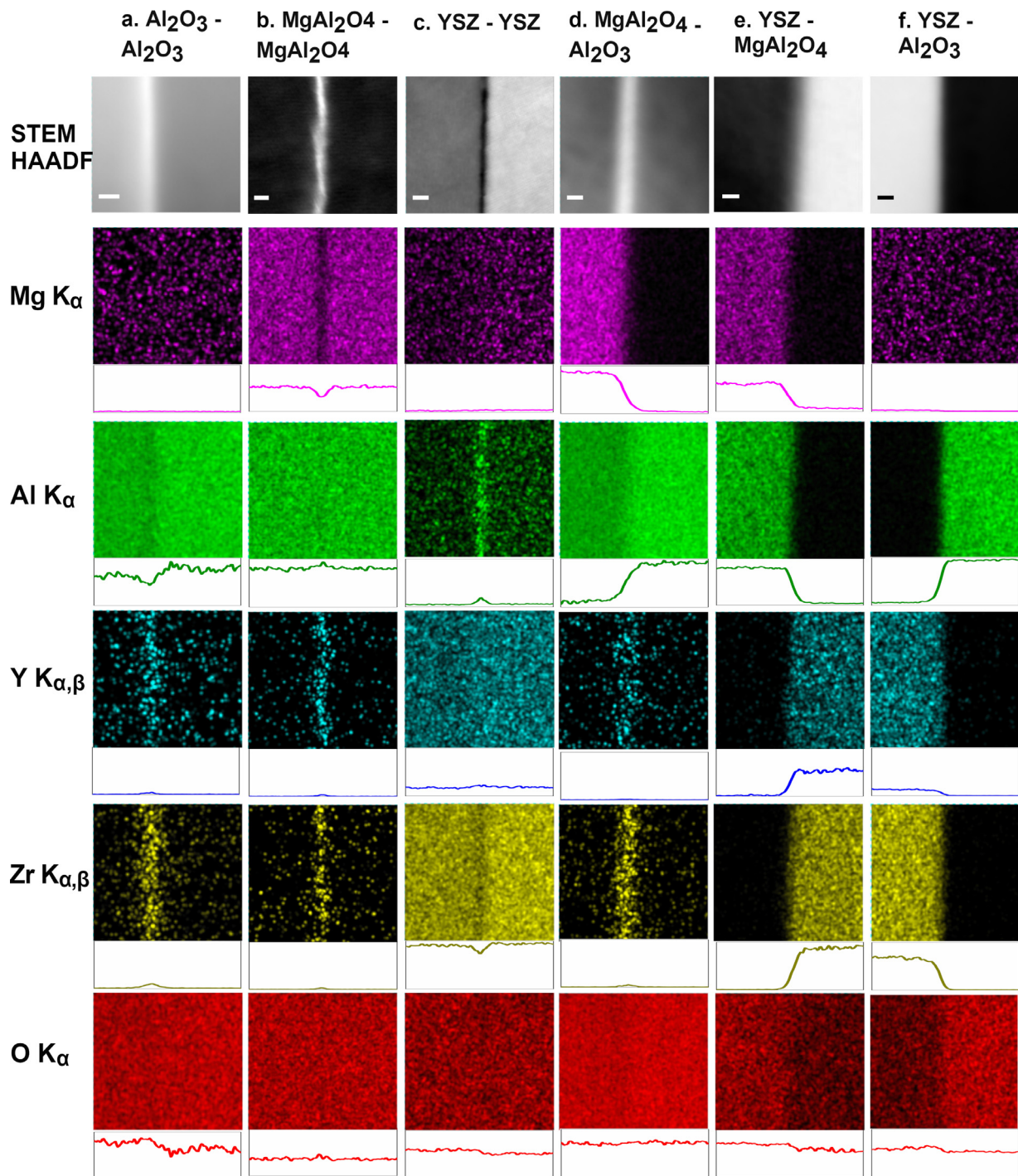
**Fig. 5.** STEM HAADF images and EDS maps for six (representative) interfaces in a flash-sintered $MgAl_2O_4$-$Al_2O_3$-YSZ ceramic. Mg $K_\alpha$, Al $K_\alpha$, Y $K_{\alpha,\beta}$, Zr $K_{\alpha,\beta}$ and O $K_\alpha$ elemental EDS maps (net counts) and their corresponding intensity profiles (net counts normalized by the total counts) are shown. Alumina-alumina grain boundary shows depletion of Al and segregation of Y/Zr (a), spinel-spinel grain boundary shows depletion of Mg and segregation of Y/Zr (b), YSZ-YSZ grain boundary shows depletion of Zr and segregation of Al (c), spinel-alumina grain boundary shows segregation of Y/Zr (d), and YSZ-spinel and YSZ-alumina interfaces do not show any segregation (e-f). Scale bar is 2nm.

ies based on dissimilar phases, a dopant/alloying element added to the metal segregates to lower the total grain boundary energy. In our oxide-oxide interface system, we observe a lack of segregation at YSZ-spinel and YSZ-alumina heterointerfaces, interpreted to meaning that for these heterointerfaces cations can be accommodated in grains on either side of the interface. Grain boundary energies for this system will be studied in future work.

The STEM HAADF images in Fig. 4 are qualitatively representative of all the sintered samples. Our results show that the elemental segregation observed at any particular type of interface—whether it is alumina-alumina, spinel-spinel, YSZ-YSZ or spinel-alumina—is qualitatively similar across the four different sintered samples analyzed. This indicates a key result of this study that the elemental segregation at grain bound-
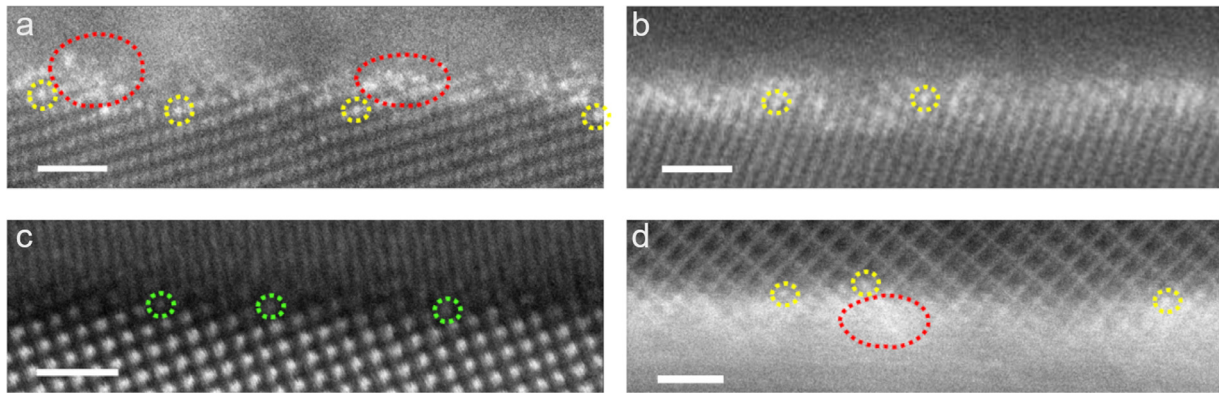
**Fig. 6.** Experimental HAADF images showing the different types of segregations observed in a three-phase system at the alumina-alumina (a), spinel-spinel (b), YSZ-YSZ (c), and spinel (top)-alumina (bottom) (d) interfaces. The scale bar is 1nm. Yellow markers highlight Y/Zr segregants and green markers highlight likely Al segregants, substituting for the matrix cations sites. Red markers highlight clustered Y/Zr segregation.

aries likely does not depend on the type of sintering, but mainly on sample composition.

Fig. 5 shows STEM HAADF images of the six types of interfaces in a flash-sintered sample and corresponding EDS elemental maps and intensity line profiles for Mg, Al, Y, Zr and O. The line profiles are shown below each EDS elemental map, with counts normalized with respect to the total counts and integrated parallel to grain boundary, as in [24]. The y-bounds for the line profiles are the same within each column in Fig. 5. Alumina-alumina grain boundary shows segregation of Y and Zr with depletion of Al counts with respect to the bulk (Fig. 5a). Spinel-spinel boundary also shows segregation of Y/Zr with a prominent depletion of Mg (Fig. 5b). YSZ-YSZ grain boundary shows a decrease in Zr counts accompanied by segregation of Al (Fig. 5c). Like spinel-spinel and alumina-alumina grain boundaries, spinel-alumina is also shown to have Y/Zr segregation (Fig. 5d). On the other hand, YSZ-spinel and YSZ-alumina interfaces do not show any elemental segregation indicating there is no driving force for cation segregation to occur; thus, these boundaries are thermodynamically stable (Fig. 5e,f).

Y and Zr segregation at alumina-alumina, spinel-spinel and spinel-alumina grain boundaries: Y and Zr cations segregate at alumina-alumina, spinel-spinel and spinel-alumina grain boundaries during grain growth in sintering likely due to negligible to low solubility of Zr and Y in spinel and alumina phases for the temperatures used in this study [49–56]. Gulgun et al. [49] studied in detail the effect of doping Y and Zr in a single-phase $\alpha$-$Al_2O_3$ system and reported that Y and Zr both segregate to the alumina-alumina grain boundaries and behave almost similarly by competing for similar sites. Similarly, Zr enrichment at grain boundaries was confirmed by Trunec et al. [57] while studying a system of Zr-doped alumina. Mohan et al. [51] also discussed Zr segregation at spinel grain boundaries (with addition of zirconia) limiting grain growth and grain boundary migration. On the other hand, Rufner et al. [58] observed enrichment of Al at spinel-spinel grain boundaries (undoped spinel) resulting in reduced Mg/Al ratio at the interface. Nuns et al. [59] also reported previously the enrichment of Al and O at spinel-spinel boundaries (in undoped sample) while Mg was found to be depleted. In our 3-phase sample at spinel-spinel boundaries, Mg is confirmed to be depleted and Y/Zr are present at the interface, while Al signal is relatively unchanged (Fig. 5b). This is one example (more discussed below) showing how grain boundary segregation in single phase ceramics can be distinct from segregation in multiphase systems.

Alumina is well-known for adsorption layers at its grain boundaries [60–62]. Unlike the adsorption of two atomic layers of Nd at Nd-doped polycrystalline alumina grain boundaries studied by Dillon and Harmer [61], our Fig. 6a shows discontinuous, slightly clustered segregation over several atomic layers at the alumina-alumina grain boundaries. Based on the EDS mapping in Fig. 5a, we know that $Y^{3+}$ and $Zr^{4+}$ segre-

gate at these grain boundaries. In Fig. 6a, it shows that some segregant cations are directly substituting the matrix cation ($Al^{3+}$) sites in the bottom alumina grain as can be seen easily due to intense Z-contrast (see yellow markings), while some other regions indicate likely adsorption of clustered Y/Zr segregants (see red markings) near the top alumina grain.

Spinel, similar to YSZ (discussed in the next sub-section), has been studied previously for space charge layers at the grain boundaries. Nuns et al. [59] explained the negatively charged grain boundary cores in spinel due to excess of Mg vacancies. Our EDS maps in Fig. 5b confirm depletion of Mg at the spinel-spinel grain boundaries which explains the segregation of Y/Zr cations for charge compensation. Since the bottom spinel grain in Fig. 6b is oriented well to zone axis, unlike the top grain, it is easy to see the segregants substituting the matrix cation sites in the bottom grain.

Similar to the case in Fig. 6a and b, only one side of the spinel-alumina grain boundary is atomically resolved (Fig. 6d) since it is generally difficult to observe a random boundary in polycrystalline samples where both the grains are aligned with respect to a zone axis. However, it is clear that segregant cations are substituting the matrix sites on to the face of the spinel (top) grain (see yellow markings in Fig. 6d). It can also be seen due to the high Z-contrast (red markings) that there are segregants present near the bottom alumina grain; however, the exact position of the segregants in this region is hard to determine due to misalignment of the bottom grain but the segregants appear more clustered.

Al segregation at YSZ-YSZ grain boundaries: Y segregation at YSZ-YSZ grain boundaries has been previously studied in single-phase YSZ systems [24,30]. However, our results indicate that in multiphase systems, grain boundary segregation behavior can be quite different than single phase systems commonly studied, which would have a direct effect on material properties. At YSZ-YSZ grain boundaries in our 3-phase samples, we observe with EDS mapping Al segregation instead of Y, accompanied by decrease in Zr (Fig. 5c). In a study conducted by Matsui et al. [33] on $Al_2O_3$-doped tetragonal polycrystalline YSZ prepared using conventional sintering, the authors found both Y and Al segregated at YSZ-YSZ boundaries. Thus, our study signifies important distinctions between the cation segregation in multi-phase system (only Al segregates) and that of un-doped YSZ [24,30] (wherein Y segregates) and Al-doped YSZ [33,63] (both Y and Al segregate). This is an important observation suggesting that the presence of other phases in the system can have a strong effect in determining the grain boundary chemistry.

According to the classical space charge theory [32], YSZ grain boundary core is predicted to be positive because of intrinsic O vacancies and possibly Zr interstitials, as explained in detail by Feng et al. [24]. This can explain the common observation of Y segregation at grain
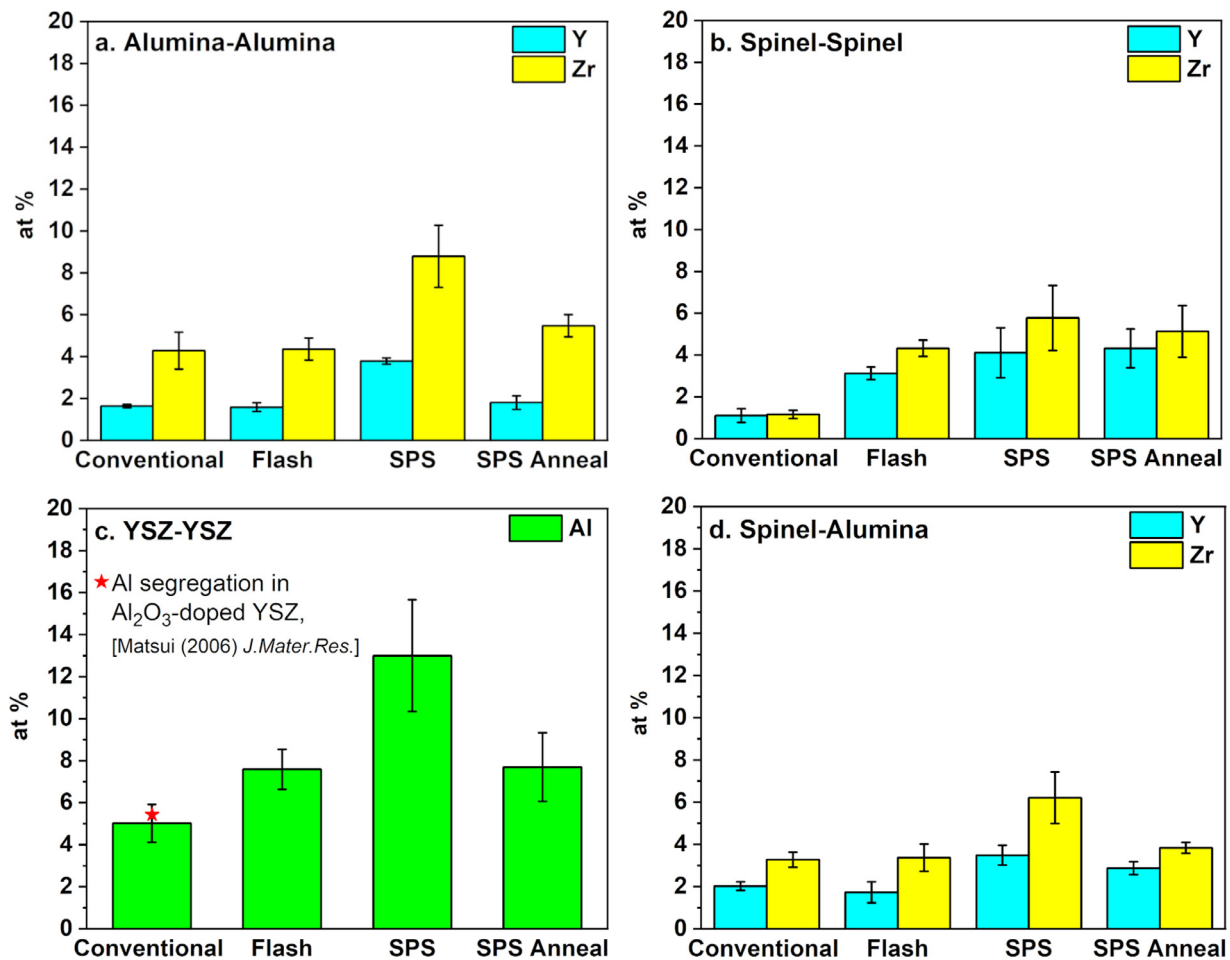
**Fig. 7.** Peak concentrations (at%) of segregated cations at different grain boundaries of conventional sintered, flash sintered, SPS and SPS anneal samples. (a,b,d) Peak concentrations of segregated Y and Zr at alumina-alumina, spinel-spinel and spinel-alumina grain boundaries respectively. (c) Peak concentrations of segregated Al at YSZ-YSZ grain boundaries for all the samples.

boundaries in single phase YSZ, where $Y^{3+}$ substitutes $Z^{4+}$ creating a net negatively charged substitutional point defect. Interestingly for our 3-phase system, the differences in ionic size between $Zr^{4+}$ and $Y^{3+}$ or $Zr^{4+}$ and $Al^{3+}$ are very similar (assuming the same coordination) [64], even though $Y^{3+}$ is larger and $Al^{3+}$ is smaller than $Zr^{4+}$. It is possible that the intensity reduction at YSZ-YSZ interface (Fig. 6c) is due to structural disorder caused by O vacancies near cation columns; however, similar contrast can be caused by cation vacancies or light element substitution in HAADF imaging [44].

Based on EDS mapping results (Fig. 5c), we know that Al is segregating while Zr is depleting at YSZ-YSZ grain boundaries. Thus, in our case we suspect that the $Al^{3+}$ cations are substituting the $Zr^{4+}$ sites (see green markings in Fig. 6c) to maintain charge balance (with oxygen vacancies), while $Y^{3+}$ stays in the YSZ grain. This interpretation is based on lower atomic number of Al compared to Zr, thus $Al^{3+}$ substitution at YSZ-YSZ grain boundary will result in lower Z-contrast as seen in Fig. 6c. This is consistent with the very low solubility of $Al^{3+}$ in YSZ [53,65,66], which would preclude $Al^{3+}$ solution in YSZ. This phenomenon of $Al^{3+}$ grain boundary defect chemistry in our 3-phase ceramic is another significant distinction between segregation behavior compared to single-phase YSZ.

Here, it is important to state that a decrease or increase in counts at the grain boundary does not necessarily mean decrease or increase in elemental concentration. The change in counts at the grain boundary core could be due to several reasons, such as thickness or density variations at the grain boundary as well as possibility of preferential

ion milling at grain boundaries by FIB sample preparation. However, results by Feng *et al.* [24] on single-phase 8YSZ shows direct correlation between increase/decrease of counts to increase/decrease of concentrations for cations (Y, Zr). Thus, in order to better understand the segregation behavior at spinel-spinel, alumina-alumina, YSZ-YSZ and spinel-alumina boundaries for the differently sintered samples, quantitative analysis was performed, and results are discussed in next section.

### 3.2. Quantitative correlations of elemental segregation at grain boundaries

In order to better correlate the sintering technique to grain boundary segregation, concentrations of segregated cations were calculated using the Cliff-Lorimer method [27,36,37]. The peak segregation concentrations at the different grain boundaries were calculated using the EDS peak intensities and averaged for 2-5 boundaries of spinel-spinel, alumina-alumina, YSZ-YSZ, and spinel-alumina for each sintered sample.

Fig. 7 shows averaged peak concentrations of Y and Zr at alumina-alumina, spinel-spinel and spinel-alumina boundaries, and Al concentration at YSZ-YSZ boundaries for all the sintered samples. The error bars represent the standard deviation of the mean segregation concentration measured for the different grain boundaries (Figs. 7 and 8). The quantitative results of Fig. 7 indicate two main points:

a. The peak Al segregation concentration (at%) at YSZ-YSZ boundaries is on average higher in the SPS sample compard to all other
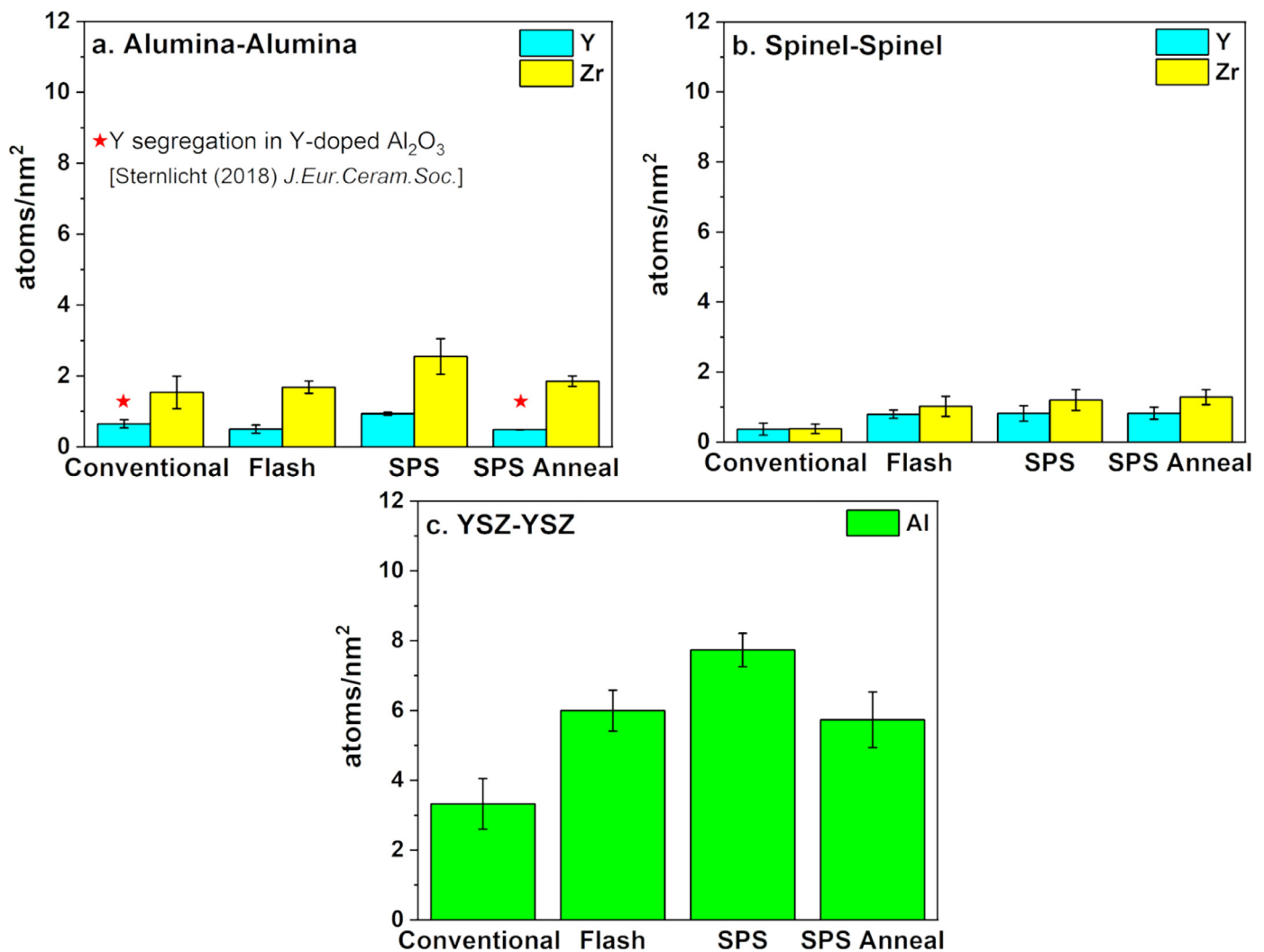
**Fig. 8.** Excess of segregated cations (atoms/nm$^2$) at grain boundaries between similar phases. (a) Y/Zr excess at alumina-alumina grain boundaries, (b) Y/Zr excess at spinel-spinel grain boundaries, and (c) Al excess at YSZ-YSZ grain boundaries.

samples (Fig. 7c). Al is known to have very limited solubility in YSZ 53,65–68]. Since solubility generally increases with increasing temperature, it is not surprising that SPS (950°C) would have relatively higher Al segregation concentration compared to conventional (1550°C) and flash (~1700°C, *in-situ*) samples. For our conventionally sintered sample (1550 °C), we measured 5.0 ± 0.9 at% Al peak concentration at the YSZ-YSZ grain boundaries (Fig. 7c). In a study conducted by Matsui *et al.* [33] on alumina-doped tetragonal YSZ, they measured ~5.4 at% Al (reported ~2.7 mol% $Al_2O_3$) segregated at the YSZ-YSZ grain boundaries in their conventionally sintered sample (1500 °C); see red marker in Fig. 7c. Their measured Al peak content at the YSZ-YSZ grain boundaries is in very good agreement with our results, despite slight differences in the processing temperature and time. However, as discussed earlier, a critical difference in the two studies is that we only observe Al segregation in our three-phase system, while both Y and Al segregation was observed by Matsui *et al.* [33] in the alumina-doped YSZ system.

b. Y and Zr concentrations in the SPS sample are found to be higher on average compared to conventional sample (Fig. 7 a,b,d). This is likely because the SPS sample was processed at the lowest temperature compared to other samples and it is also a rapid sintering technique, thus resulting in higher-energy non-equilibrium grain boundaries with higher segregation. On the other hand, the segregation concentrations in flash and SPS anneal samples are consistently sim-

ilar to each other which is an interesting observation considering the difference in processing parameters (time, temperature etc.) of these samples. This suggests that very high temperatures reached during flash sintering results in similar segregation concentrations compared to a sample annealed for several hours at lower temperature. For the alumina-alumina boundary (Fig. 7a), the average peak concentrations of Y and Zr segregants in flash and SPS anneal samples are similar to the conventional sample. However, in the spinel-spinel case, the flash and SPS anneal samples are similar to the SPS sample; the conventional sample shows relatively lower peak concentrations of segregants. This suggests that the segregation trends can vary for different boundaries likely depending on the type of segregation occuring.

To compare our results with similar material systems studied by other researchers [39,40], the excess of segregated species (atoms/nm$^2$) is also calculated for the homointerfaces YSZ-YSZ, spinel-spinel and alumina-alumina (Fig. 8). While we do expect grain boundary anisotropy to produce a distribution in segregation from boundary to boundary, some important correlations can still be drawn from the mean excess of segregated cations. Similar to the atomic% peak concentrations at alumina-alumina boundaries (Fig. 7a), mean excess concentrations of Y/Zr for SPS sample are higher than the other samples (Fig. 8a). Similarly, for spinel-spinel case, the conventional sample has the lowest
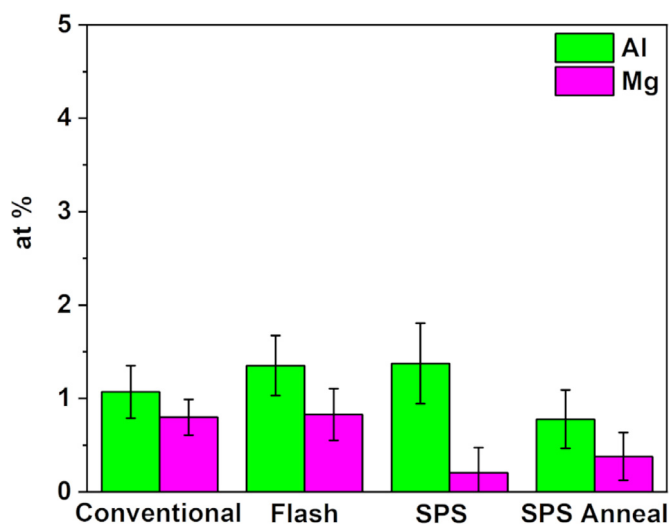
**Fig. 9.** Average concentration (at%) of Mg and Al in YSZ grains.

mean excess of Y and Zr (Fig. 8b), just like we observed in Fig. 7b. Lastly, for YSZ-YSZ boundaries, mean Al excess is the lowest for conventional sample (Fig. 8c), similar to the observation in Fig. 7c. In short, we conclude from our quantitative analysis that the conventional sample shows relatively lower excess of segregated cations compared to SPS sample, while the flash and SPS anneal samples vary in trends from boundary to boundary.

Sternlicht *et al.* [39] reported the amount of Y excess (atoms/nm$^2$) at the grain boundaries of a Y-doped alumina system with bi-modal structure; their sample was processed by SPS in two steps and then annealed (1500°C for 4 h). Considering the type of sintering, temperatures and times of processing described in their work [39], our conventional and SPS anneal samples of this study were chosen for comparison. They reported a mean Y excess of 1.3 atoms/nm$^2$ at the alumina-alumina grain boundaries between smaller grains (red markings on Fig. 8a), which is suitable for comparison to our study. In the conventional sintered sample, we determined mean Y excess of 0.7 atoms/nm$^2$ and mean Zr excess of 1.5 atoms/nm$^2$ at the alumina-alumina grain boundaries (Fig. 8a). For the SPS anneal sample, we determined mean Y excess of 0.5 atoms/nm$^2$ and mean Zr excess of 1.9 atoms/nm$^2$ (Fig. 8a). Since both Y and Zr segregated at alumina-alumina boundaries in our 3-phase system, our results for conventional and SPS anneal samples are in good agreement with the previous report of Y segregation at Y-doped alumina grain boundaries by Sternlicht *et al.* [39], considering differences in starting materials and overall processing. Overall, our quantitative results correlate different sintering processes with resulting elemental segregation and compositional inhomogeneity at grain boundaries, which can have a strong impact on many material properties [9,19–21,28,29].

### 3.3. Measured concentrations of segregated cations within the grains

Al (from Al$_2$O$_3$) is known to have very limited solubility in cubic YSZ, reported as <1 mol% (or <0.9 at% considering cations only) at 1600 °C 53,65–68]. While Mg did not segregate to YSZ-YSZ grain boundaries, we analyzed its concentration in YSZ grains, along with Al. Solubility of Mg in cubic YSZ (in experiments reacting MgO and YSZ) has been reported to be much more considerable up to 10 mol% (~9.3 at% considering cations only) [69,70]. Considering cations only, Mg from MgO starts with 100 at% as it goes into YSZ; however, the phase in our material system is MgAl$_2$O$_4$ which makes the initial Mg content to be only 33 at%. Considering this, we calculated average concentrations of Mg and Al in estimated center of eight YSZ grains in all four sintered samples using EDS spot analysis (Fig. 9). The error bars represent the standard deviation of the mean concentration measured for the different grains.

The average concentrations of both Mg and Al in YSZ grains for all sintered samples, measured using EDS spot analysis, were calculated to be approximately <1.5 at%. The average concentrations of Mg in YSZ grains for all four sintered samples are lower than Al concentrations, which is the opposite trend to what we initially expected based on previous literature [53,65,69]. The measured concentration of Al in YSZ is statistically the same for all four differently processed samples. The solubility of Al is commonly known to be negligible below 1200 °C [71,72]. While the SPS sample was sintered at 950°C and annealed at 1000°C for 1 h, the actual sample temperature is expected to have reached higher than the furnace temperature because SPS is a current-assisted sintering technique (applied current + pressure) [73,74]. Our results suggest that Al is hindering the solubility of Mg in YSZ grains, while the presence of Mg is assisting to increase the solubility of Al. This phenomenon is similar to what was reported recently for Ca and Mg co-doped alumina system. Moshe and Kaplan [75] reported an increase in solubility limit of Mg in alumina in the presence of Ca compared to just Mg-doped alumina. Similarly, they reported a decrease in solubility limit of Ca in the presence of Mg compared to just Ca-doped alumina [75]. We suspect that the presence of Al in the YSZ grain lowers the Mg solubility, which lowers the thermodynamic driving force for Mg diffusion into the YSZ grains.

Solubility of Y and Zr in spinel and alumina phases have been reported to be quite limited for the temperature range studied here. Solubility of Y in alumina has been reported under a wide range, from <10 ppm up to 200 ppm (0.001-0.02%) [54,55]. Solubility of Y and Zr in spinel has been reported to be very limited [51,76]. The solubility of Zr in alumina has also been reported to be quite low ~ 500-1000 ppm (0.05-0.1%) [56]. In order to confirm that the concentrations of Y and Zr in spinel and alumina grains of our 3-phase samples are in good agreement with previous literature, we performed spot EDS analysis at the centers of three spinel and alumina grains for conventional, flash and SPS samples. The averaged concentrations of Y in spinel and alumina grains were calculated to be ≤ 0.08 at%, which is negligible based on limitations of EDS detection around 0.1%. Similarly, the average concentrations of Zr in spinel and alumina grains were calculated to be very low ≤0.15 at%.

Besides measuring concentrations of segregated cations at grain boundaries and in bulk, we also analyzed variation of Al/Mg ratio in the spinel phase of our 3-phase systems. Spinel is known to exhibit significant deviations from stoichiometry (MgAl$_2$O$_4$), especially with increasing sintering and annealing temperatures. Kok *et al.* [34] previously showed (in same 3-phase composition used in this study) that Al/Mg ratio in spinel varies considerably due to very high temperatures reached during flash sintering. They showed that it is possible to form a single-phase high-alumina spinel, and reported that different compositions of non-stoichiometric spinel can form during the heat treatment. Using EDS mapping, we calculated average Al:Mg ratios (unitless) in spinel grains of all four samples: 3.0±0.04 (flash), 2.8±0.07 (conventional), 2.5±0.11 (SPS anneal) and 2.3±0.11 (SPS). Compared to the standard 2:1 Al:Mg ratio in stoichiometric spinel, the Al:Mg ratio in spinel grains of the SPS sample (sintered at lowest T~950 °C) show the smallest deviation, whereas spinel grains in the flash sample (*in-situ* T~1700 °C) show the greatest deviation. These observations that deviations from stoichiometry correlate with increasing processing temperature is in agreement with the phase diagram [77].

### 3.4. Role of grain size variation on grain boundary segregation

It is known that grain size can play a critical role in grain boundary segregation phenomena, both in metals and ceramic systems. Similar to the limitations in grain boundary segregation studies, most studies focusing on grain size effects are based on doped systems [78–81]. Gruffel and Carry [78] studied the Y-segregation content with respect to grain size in Y-doped alumina and observed that the trend depends on the initial dopant concentration. When doping with lower concentrations of

$Y_2O_3$ (500 ppm wt.), they observed the segregation content increased linearly with grain size. On the other hand, when doping with 1500 ppm wt. $Y_2O_3$, the grain boundaries were saturated with yttrium and grain boundary composition was independent of grain size (studied for 800 nm to ~3.5 μm grain sizes) [78]. Aoki et al. also concluded that grain boundary coverage (atoms/area) increases with increasing grain size in CaO-stabilized $ZrO_2$ (containing different impurity solutes like Si) until the saturation of total solute is reached ~ 1 monolayer. On the other hand, Stemmer et al. [82] found strong Y segregation in tetragonal YSZ grain boundaries, regardless of varying grain sizes and impurity levels.

The above discussion shows that grain size can have a huge impact on grain boundary segregation behavior in single-phase ceramics. In our sintered three-phase samples, the situation is more complex because they are made with equal volume percent (33%) of YSZ, alumina and spinel. Thus, there are, effectively, infinite sources of ions in each sample which can segregate to, or cover *via* diffusion from another phase, the grain boundaries. It may, therefore, be appropriate to imagine our materials as being heavily-doped, i.e., as having a very large number of available segregants. In this case, we would compare our results with those of Gruffel and Carry [78], who found that grain boundary composition was independent of grain size when doping with 1500 ppm wt. $Y_2O_3$.

## 4. Conclusions

Grain boundary segregation behavior in multiphase systems was shown to have important distinction compared to single-phase systems (doped and undoped) commonly studied. It was determined that the presence of other phases in the system can have a strong effect on final grain boundary chemistry. For all sintering processes, Y and Zr was found to segregate at spinel-spinel, alumina-alumina, and spinel-alumina grain boundaries, while Al was found to segregate at YSZ-YSZ grain boundaries. On the other hand, YSZ-spinel and YSZ-alumina heterointerfaces did not show any cation segregation. This suggests that the cations (Y, Zr, Al, Mg) prefer to exist in the grains on either side of the interface, and indicates that segregation would most likely increase the interfacial energy. The segregants at alumina-alumina boundaries were shown to both substitute the matrix sites as well as adsorb as clusters, while the spinel-spinel and YSZ-YSZ boundaries appeared to have segregants substituting the matrix cation sites. For all the interfaces showing segregation, our SPS sample showed relatively higher average grain boundary segregation compared to the conventional sintered sample, suggesting rapid sintering at low temperatures results in higher grain boundary segregation. The grain boundary segregation concentrations for the flash sintered sample were consistently found to be similar to the SPS anneal sample which was an interesting observation in this study. This suggests that very high temperatures reached during flash sintering results in similar grain boundary concentrations compared to a sample annealed for several hours at lower temperature.

Our results also highlight the concentrations of segregated cations within the three phases and indicate that Al and Mg are possibly acting as competing cations to diffuse in the YSZ grains. The qualitative and quantitative results correlate grain boundary segregation behavior to the different sintering techniques, which may be a beneficial guide to understand grain boundary segregation for other technical systems and how this segregation relates to material properties, such as thermal and electrical conductivity, and fracture.

## Declaration of Competing Interest

The authors declare that they have no known competing financial interests or personal relationships that could have appeared to influence the work reported in this paper.

## References

[1] T. Watanabe, S. Tsurekawa, Toughening of brittle materials by grain boundary engineering, Mater. Sci. Eng. A 387–389 (2004) 447–455.

[2] R.L. Coble, A Model for Boundary Diffusion Controlled Creep in Polycrystalline Materials, J, Appl. Phys. 34 (1963) 1679–1682.

[3] H. Dong, B. Wen, R. Melnik, Relative importance of grain boundaries and size effects in thermal conductivity of nanocrystalline materials, Sci. Rep. 4 (2014) 7037.

[4] W.C. Johnson, Grain boundary segregation in ceramics, Met. Trans A. 8 (1977) 1413–1422.

[5] J.F. Nie, Y.M. Zhu, J.Z. Liu, X.Y. Fang, Periodic segregation of solute atoms in fully coherent twin boundaries, Science 340 (2013) 957–960.

[6] J.P. Buban, K. Matsunaga, J. Chen, N. Shibata, W.Y. Ching, T. Yamamoto, Y. Ikuhara, Grain boundary strengthening in alumina by rare earth impurities, Science 311 (2006) 212–215.

[7] B. Feng, I. Sugiyama, H. Hojo, H. Ohta, N. Shibata, Y. Ikuhara, Atomic structures and oxygen dynamics of $CeO_2$ grain boundaries, Sci. Rep (2016).

[8] Y. Sato, J.P. Buban, T. Mizoguchi, N. Shibata, M. Yodogawa, T. Yamamoto, Y. Ikuhara, Role of Pr segregation in acceptor-state formation at ZnO Grain Boundaries, Phys. Rev. Lett. 97 (2006) 106802.

[9] N. Goel, E. Webb III, A. Oztekin, J. Rickman, S. Neti, Kapitza resistance at segregated boundaries in $β$-SiC, J. Appl. Phys. 118 (2015) 115101.

[10] G.S. Rohrer, Grain boundary energy anisotropy: a review, J. Mater. Sci. 46 (2011) 5881–5895.

[11] P. Wynblatt, G.S. Rohrer, F. Papillon, Grain boundary segregation in oxide ceramics, J. Eur. Ceram. Soc. 23 (2003) 2841–2848.

[12] M. Cologna, A.L.G. Prette, R. Raj, Flash-Sintering of Cubic Yttria-Stabilized Zirconia at 750°C for Possible Use in SOFC Manufacturing, J. Am. Ceram. Soc. 94 (2011) 316–319.

[13] D. Kok, S.K. Jha, R. Raj, M.L. Mecartney, Flash sintering of a three-phase alumina, spinel, and yttria-stabilized zirconia composite, J. Am. Ceram. Soc. 100 (2017) 3262–3268.

[14] J.P. Kelly, O.A. Graeve, Spark plasma sintering as an approach to manufacture bulk materials: feasibility and cost savings, JOM 67 (2015) 29–33.

[15] J.S.C. Francis, R. Raj, Influence of the field and the current limit on flash sintering at isothermal furnace temperatures, J. Am. Ceram. Soc. 96 (2013) 2754–2758.

[16] M. Biesuz, V.M. Sglavo, Flash sintering of ceramics, J. Eur. Ceram. Soc. 39 (2019) 115–143.

[17] Z.A. Munir, U. Anselmi-Tamburini, M. Ohyanagi, The effect of electric field and pressure on the synthesis and consolidation of materials: A review of the spark plasma sintering method, J. Mater. Sci. 41 (2006) 763–777.

[18] T. Kinoshita, S. Munekawa, Effect of grain boundary segregation on thermal conductivity of hot-pressed silicon carbide, Acta Mater 45 (1997) 2001–2012.

[19] N. Farahi, S. Prabhudev, M. Bugnet, G.A. Botton, J.R. Salvador, H. Kleinke, Effect of silicon carbide nanoparticles on the grain boundary segregation and thermoelectric properties of bismuth doped $Mg_2Si_{0.7}Ge_{0.3}$, J. Electron. Mater. 45 (2016) 6052–6058.

[20] W. Cao, A. Kundu, Z. Yu, M.P. Harmer, R.P. Vinci, Direct correlations between fracture toughness and grain boundary segregation behavior in ytterbium-doped magnesium aluminate spinel, Scr. Mater. 69 (2013) 81–84.

[21] R.L. Satet, M.J. Hoffmann, Influence of the rare-earth element on the mechanical properties of Re–Mg–Bearing Silicon Nitride, J. Am. Ceram. Soc. 88 (2005) 2485–2490.

[22] J.P. Buban, K. Matsunaga, J. Chen, N. Shibata, W.Y. Ching, T. Yamamoto, Y. Ikuhara, Grain boundary strengthening in alumina by rare earth impurities, Science 311 (2006) 212–215.

[23] G.D. West, J.M. Perkins, M.H. Lewis, The effect of rare earth dopants on grain boundary cohesion in alumina, J. Eur. Ceram. Soc. 27 (2007) 1913–1918.

[24] B. Feng, N.R. Lugg, A. Kumamoto, Y. Ikuhara, N. Shibata, Direct observation of oxygen vacancy distribution across yttria-stabilized zirconia grain boundaries, ACS Nano 11 (2017) 11376–11382.

[25] N. Shibata, G.S. Painter, R.L. Satet, M.J. Hoffmann, S.J. Pennycook, P.F. Becher, Rare-earth adsorption at intergranular interfaces in silicon nitride ceramics: Sub-nanometer observations and theory, Phys. Rev. B. 72 (2005) 140101.

[26] B. Feng, T. Yokoi, A. Kumamoto, M. Yoshiya, Y. Ikuhara, N. Shibata, Atomically ordered solute segregation behaviour in an oxide grain boundary, Nat. Commun. 7 (2016) 1–6.

[27] W.J. Bowman, A. Darbal, P.A. Crozier, Linking Macroscopic and nanoscopic ionic conductivity: a semiempirical framework for characterizing grain boundary conductivity in polycrystalline ceramics, ACS Appl. Mater. Interfaces. 12 (2020) 507–517.

[28] W.J. Bowman, J. Zhu, R. Sharma, P.A. Crozier, Electrical conductivity and grain boundary composition of Gd-doped and Gd/Pr co-doped ceria, Solid State Ion 272 (2015) 9–17.

[29] W.J. Bowman, M.N. Kelly, G.S. Rohrer, C.A. Hernandez, P.A. Crozier, Enhanced ionic conductivity in electroceramics by nanoscale enrichment of grain boundaries with high solute concentration, Nanoscale 9 (2017) 17293–17302.

[30] N. Shibata, F. Oba, T. Yamamoto, Y. Ikuhara, Structure, energy and solute segregation behaviour of [110]symmetric tilt grain boundaries in yttria-stabilized cubic zirconia, Philos. Mag. 84 (2004) 2381–2415.

[31] K. Matsui, H. Yoshida, Y. Ikuhara, Grain-boundary structure and microstructure development mechanism in 2–8mol% yttria-stabilized zirconia polycrystals, Acta Mater 56 (2008) 1315–1325.

[32] K.L. Kliewer, J.S. Koehler, Space Charge in Ionic Crystals. I. general approach with application to NaCl, Phys. Rev. 140 (1965) A1226–A1240.

[33] K. Matsui, N. Ohmichi, M. Ohgai, H. Yoshida, Y. Ikuhara, Effect of alumina-doping on grain boundary segregation-induced phase transformation in yttria-stabilized tetragonal zirconia polycrystal, J. Mater. Res. 21 (2006) 2278–2289.

[34] D. Kok, D. Yadav, E. Sortino, S.J. McCormack, K.-P. Tseng, W.M. Kriven, R. Raj, M.L. Mecartney, $\alpha$-Alumina and spinel react into single-phase high-alumina spinel in <3 seconds during flash sintering, J. Am. Ceram. Soc. 102 (2019) 644–653.

[35] K.K. Ohtaki, M.K. Patel, M.L. Crespillo, K.K. Karandikar, Y. Zhang, O.A. Graeve, M.L. Mecartney, Improved high temperature radiation damage tolerance in a three-phase ceramic with heterointerfaces, Sci. Rep. 8 (2018) 13993.

[36] G.W. Lorimer, Quantitative X-ray microanalysis of thin specimens in the transmission electron microscope; a review, Mineral. Mag. 51 (1987) 49–60.

[37] G. Cliff, G.W. Lorimer, The quantitative analysis of thin specimens, J. Microsc 103 (1975) 203–207.

[38] D.B. Williams, C.B. Carter, Quantitative X-ray Analysis, in: D.B. Williams, C.B. Carter (Eds.), Transmission Electron Microscopy. A Textbook for Materials Science, Springer, US, Boston, MA, 2009, pp. 639–662.

[39] H. Sternlicht, S.A. Bojarski, G.S. Rohrer, W.D. Kaplan, Quantitative differences in the Y grain boundary excess at boundaries delimiting large and small grains in Y doped $Al_2O_3$, J. Eur. Ceram. Soc. 38 (2018) 1829–1835.

[40] X.F. Zhang, Q. Yang, L.C.D. Jonghe, Z. Zhang, Energy dispersive spectroscopy analysis of aluminium segregation in silicon carbide grain boundaries, J. Microsc 207 (2002) 58–68.

[41] V.J. Keast, D.B. Williams, Quantification of boundary segregation in the analytical electron microscope, J. Microsc 199 (2000) 45–55.

[42] P. Doig, P.E.J. Flewitt, Microanalysis of grain boundary segregation in embrittled Iron-3wt% Nickel Alloys Using STEM, J. Microsc 112 (1978) 257–267.

[43] S. Pennycook, Scanning Transmission Electron Microscopy - Imaging and Analysis, Springer, http://www.springer.com/us/book/9781441971999.

[44] H.-S. Lee, S.D. Findlay, T. Mizoguchi, Y. Ikuhara, The effect of vacancies on the annular dark field image contrast of grain boundaries: A SrTiO3 case study, Ultramicroscopy 111 (2011) 1531–1539.

[45] S.D. Findlay, S. Azuma, N. Shibata, E. Okunishi, Y. Ikuhara, Direct oxygen imaging within a ceramic interface, with some observations upon the dark contrast at the grain boundary, Ultramicroscopy 111 (2011) 285–289.

[46] H. Nahor, Y. Kauffmann, W.D. Kaplan, The Cr-Doped Ni-YSZ(111) interface: Segregation, oxidation and the Ni equilibrium crystal shape, Acta Mater 166 (2019) 28–36.

[47] D.A. Shashkov, D.N. Seidman, Atomic scale studies of segregation at ceramic/metal heterophase interfaces, Phys. Rev. Lett. 75 (1995) 268–271.

[48] X. Zhang, T. Hu, J.F. Rufner, T.B. LaGrange, G.H. Campbell, E.J. Lavernia, J.M. Schoenung, K. van Benthem, Metal/ceramic interface structures and segregation behavior in aluminum-based composites, Acta Mater 95 (2015) 254–263.

[49] M.A. Gülgün, R. Voytovych, I. Maclaren, M. Rühle, R.M. Cannon, Cation Segregation in an Oxide Ceramic with Low Solubility: Yttrium Doped $\alpha$-Alumina, Interface Sci 10 (2002) 99–110.

[50] R. Sarkar, H.S. Tripathi, A. Ghosh, Reaction sintering of different spinel compositions in the presence of $Y_2O_3$, Mater. Lett. 58 (2004) 2186–2191.

[51] S.K. Mohan, R. Sarkar, Effect of $ZrO_2$ addition on $MgAl_2O_4$ spinel from commercial grade oxide reactants, Ceram. Int. 42 (2016) 10355–10365.

[52] T. Suzuki, K. Itatani, M. Aizawa, F.S. Howell, A. Kishioka, Sinterability of spinel $(MgAl_2O_4)$-Zirconia composite powder prepared by double nozzle ultrasonic spray pyrolysis, J. Eur. Ceram. Soc. 16 (1996) 1171–1178.

[53] M.A. Stough, J.R. Hellmann, Solid solubility and precipitation in a single-crystal alumina-zirconia system, J. Am. Ceram. Soc. 85 (2002) 2895–2902.

[54] S.K. Behera, Atomic structural features of dopant segregated grain boundary complexions in alumina by EXAFS, Ph.D. Thesis, Lehigh University, 2010.

[55] J.D. Cawley, J.W. Halloran, Dopant distribution in nominally yttrium-doped sapphire, J. Am. Ceram. Soc. 69 (1986) C-195-C–196.

[56] S.K. Behera, P.R. Cantwell, M.P. Harmer, A grain boundary mobility discontinuity in reactive element Zr-doped $Al_2O_3$, Scr. Mater. 90–91 (2014) 33–36.

[57] M. Trunec, K. Maca, R. Chmelik, Polycrystalline alumina ceramics doped with nanoparticles for increased transparency, J. Eur. Ceram. Soc. 35 (2015) 1001–1009.

[58] J.F. Rufner, D. Kaseman, R.H.R. Castro, K. van Benthem, DC electric field-enhanced grain-boundary mobility in magnesium aluminate during annealing, J. Am. Ceram. Soc. 99 (2016) 1951–1959.

[59] N. Nuns, F. Béclin, J. Crampon, Grain-boundary characterization in a nonstoichiometric fine-grained magnesium aluminate spinel: effects of defect segregation at the space-charge layers, J. Am. Ceram. Soc. 92 (2009) 870–875.

[60] S.J. Dillon, M.P. Harmer, Multiple grain boundary transitions in ceramics: A case study of alumina, Acta Mater 55 (2007) 5247–5254.

[61] S.J. Dillon, M.P. Harmer, Direct observation of multilayer adsorption on alumina grain boundaries, J. Am. Ceram. Soc. 90 (2007) 996–998.

[62] I. MacLaren, R.M. Cannon, M.A. Gülgün, R. Voytovych, N. Popescu-Pogrion, C. Scheu, U. Täffner, M. Rühle, Abnormal grain growth in alumina: synergistic effects of Yttria and Silica, J. Am. Ceram. Soc. 86 (2003) 650–659.

[63] S. Nazarpour, C. López-Gándara, C. Zamani, J.M. Fernández-Sanjuán, F.M. Ramos, A. Cirera, Phase transformation studies on YSZ doped with alumina. Part 2: Yttria segregation, J. Alloys Compd. 505 (2010) 534–541.

[64] R.D. Shannon, Revised effective ionic radii and systematic studies of interatomic distances in halides and chalcogenides, Acta Crystallogr. A. 32 (1976) 751–767.

[65] D. Hotza, A. Leo, J. Sunarso, J.C. Diniz da Costa, Effect of nano- $Al_2O_3$ addition on the densification of YSZ electrolytes, J. Nano Res 6 (2009) 115–122.

[66] S. Tekeli, The solid solubility limit of $Al_2O_3$ and its effect on densification and microstructural evolution in cubic-zirconia used as an electrolyte for solid oxide fuel cell, Mater. Des. 28 (2007) 713–716.

[67] E.P. Butler, J. Drennan, Microstructural analysis of sintered high-conductivity zirconia with Al2O3 Additions, J. Am. Ceram. Soc. 65 (1982) 474–478.

[68] R.H.L. Garcia, V. Ussui, N.B. de Lima, E.N.S. Muccillo, D.R.R. Lazar, Physical properties of alumina/yttria-stabilized zirconia composites with improved microstructure, J. Alloys Compd 486 (2009) 747–753.

[69] F.C. Fonseca, D.Z. de Florio, R. Muccillo, Impedance spectroscopy study of the sintering of yttria-stabilized zirconia/magnesia composites, Solid State Ion 180 (2009) 822–826.

[70] T. Bak, J. Nowotny, K. Prince, M. Rekas, C.C. Sorrell, Grain boundary diffusion of magnesium in Zirconia, J. Am. Ceram. Soc. 85 (2002) 2244–2250.

[71] E. Drożdż, The influence of the method of addition of $Al_2O_3$ to 3YSZ material on its thermal and electrical properties, J. Therm. Anal. Calorim. 118 (2014) 1345–1353.

[72] M.J. Bannister, Development of the SIRO oxygen sensor: sub-solidus phase equilibria In the system $ZrO_2$-$Al_2O_3$-$Y_2O_3$, J. Aust. Ceram. Soc. (1982) 18.

[73] D.V. Dudina, D.M. Hulbert, D. Jiang, C. Unuvar, S.J. Cytron, A.K. Mukherjee, In situ boron carbide–titanium diboride composites prepared by mechanical milling and subsequent Spark Plasma Sintering, J. Mater. Sci. 43 (2008) 3569–3576.

[74] U. Anselmi-Tamburini, Y. Kodera, M. Gasch, C. Unuvar, Z.A. Munir, M. Ohyanagi, S.M. Johnson, Synthesis and characterization of dense ultra-high temperature thermal protection materials produced by field activation through spark plasma sintering (SPS): I. Hafnium Diboride, J. Mater. Sci. 41 (2006) 3097–3104.

[75] R. Moshe, W.D. Kaplan, The combined influence of Mg and Ca on microstructural evolution of alumina, J. Am. Ceram. Soc. 102 (2019) 4882–4887.

[76] A.P. Tomsia, A.M. Glaeser, Ceramic Microstructures: Control at the Atomic Level, Springer Science & Business Media, 2012.

[77] B. Hallstedt, Thermodynamic Assessment of the System MgO–$Al_2O_3$, J. Am. Ceram. Soc. 75 (1992) 1497–1507.

[78] P. Gruffel, C. Carry, Effect of grain size on yttrium grain boundary segregation in fine-grained alumina, J. Eur. Ceram. Soc. 11 (1993) 189–199.

[79] K. Ishida, Effect of grain size on grain boundary segregation, J. Alloys Compd 235 (1996) 244–249.

[80] R.F. Cook, A.G. Schrott, Calcium segregation to grain boundaries in alumina, J. Am. Ceram. Soc. 71 (1988) 50–58.

[81] M. Aoki, Y.-M. Chiang, I. Kosacki, L.J.-R. Lee, H. Tuller, Y. Liu, Solute segregation and grain-boundary impedance in high-purity stabilized zirconia, J. Am. Ceram. Soc. 79 (1996) 1169–1180.

[82] S. Stemmer, J. Vleugels, O. Van Der Biest, Grain boundary segregation in high-purity, yttria-stabilized tetragonal zirconia polycrystals (Y-TZP), J. Eur. Ceram. Soc. 18 (1998) 1565–1570.